Infrared and Optical Properties of Carbon Nanotube Dipole Antennas

Jin Hao, *Member, IEEE*, and George W. Hanson, *Senior Member, IEEE*

***Abstract*—The characteristics of armchair carbon nanotube dipole antennas are investigated in the infrared and optical regime. The analysis is based on a classical electromagnetic Hallén's-type integral equation, and an axial quantum mechanical conductance function for the tube. It is found that, within a certain frequency span in the GHz-THz range, finite-length carbon nanotube dipoles resonate at approximately integer multiples of one-half of a plasma wavelength. Outside of this range, current resonances are strongly damped. In the optical regime, antenna properties are strongly modulated by interband transitions. General antenna characteristics of finite-length carbon nanotube dipoles are presented, such as input impedance, current profile, gain, and efficiency, and radiation patterns are discussed.**

***Index Terms*—Carbon nanotube antenna, electromagnetic theory, nanotechnology, optical antenna.**

I. Introduction

SINCE THE discovery of carbon nanotubes [1], there has been a lot of research into their fundamental properties, and much excitement concerning possible applications. Multiwall carbon nanotubes (MWNTs), single-wall carbon nanotubes (SWNTs), carbon nanotube ropes, and other structures exist, although here attention is focused on SWNTs. These tubes typically have radius values on the order of nanometers, and their lengths can range from the nanometer scale up to, currently, centimeters [2].

SWNTs can be envisioned as a rolled-up graphene sheet, which, at an atomic level, has the honeycomb structure shown in Fig. 1. The small circles denote the location of carbon atoms, and the lines depict carbon–carbon bonds [3]. Lattice basis vectors are $\mathbf{a}_1$ and $\mathbf{a}_2$ as shown, and the relative position vector is $\mathbf{R} = m\mathbf{a}_1 + n\mathbf{a}_2$, where m and n are integers. If the nanotube axis is the ξ or η axis in Fig. 1, the resulting structure is called a zigzag or armchair tube, respectively. If the carbon nanotube (CN) axis is neither the ξ nor the η axis as shown, the resulting nanotube is called a chiral CN. Therefore, carbon nanotubes can be characterized by the dual index (m, n), where $(m, 0)$ for zigzag CNs, (m, m) for armchair CNs, and (m, n), $0 < n \neq m$, for chiral nanotubes.

Electrically, carbon nanotubes can be either metallic or semiconducting, depending on their geometry (i.e., on m, n) [3], [4]. Armchair CNs are always metallic (they exhibit no energy bandgap), as are zigzag CNs with $m = 3q$, where q is an integer (although zigzag tubes can have a small bandgap due to curvature effects, one can usually consider them as metallic from an applications perspective). The resulting cross-sectional radius of a carbon nanotube is given by [3]

$$a = \frac{\sqrt{3}}{2\pi} b \sqrt{m^2 + mn + n^2} \tag{1}$$

where $b = 0.142$ nm is the interatomic distance in graphene.

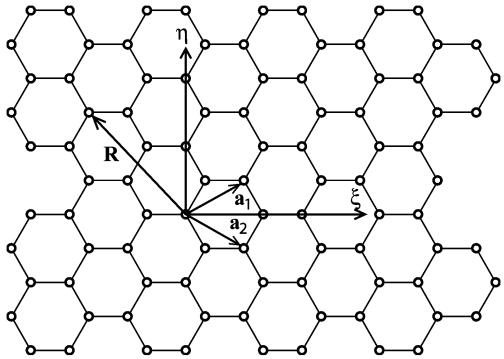

Fig. 1. Graphene sheet showing coordinate system.

Much of the excitement concerning carbon nanotubes has centered around their possible use as transistors [5], [6], as field emission devices [7], as sensors [8], and in other electronic applications. In this work we investigate the possible application of a carbon nanotube as an antenna element. Although there has been little activity in this area, some work has been done to gauge the suitability of CNs for antenna applications. In [9], carbon nanotube antennas were studied using a transmission-line model, where several effects were noted: in particular, since the wave velocity on a carbon nanotube transmission line is on the order of the Fermi velocity v_F, rather than the speed of light c, and since $v_F \ll c$, wavelengths are therefore much shorter on a carbon nanotube compared to on a typical macroscopic metallic tube or cylinder. In [10], finite-length dipole antennas formed by carbon nanotubes were investigated using a Hallén's-type integral equation (IE), where the input impedance, current profile, and efficiency were presented. In [11], an infinite-length carbon nanotube dipole antenna was studied using Fourier transform techniques.

Both [10] and [11] concerned carbon nanotube antennas in the GHz and low THz regime. In [12] the Leontovich–Levin integrodifferential equation was developed for CNs and applied in the optical range. In that work, both approximate analytical and numerical solutions were provided for optical scattering from finite-length tubes. Finally, measurements on a parallel array of

Manuscript received December 4, 2005; revised July 7, 2006. The review of this paper was arranged by Associate Editor T. Hiramoto.

J. Hao is with the Department of Electrical Engineering, University of Wisconsin-Milwaukee, Milwaukee, WI 53211 USA.

G. W. Hanson is with the University of Wisconsin-Milwaukee, Milwaukee, WI 53211 USA.

Color versions of Figs. 3–12 are available online at http://ieeexplore.ieee.org.

Digital Object Identifier 10.1109/TNANO.2006.883475

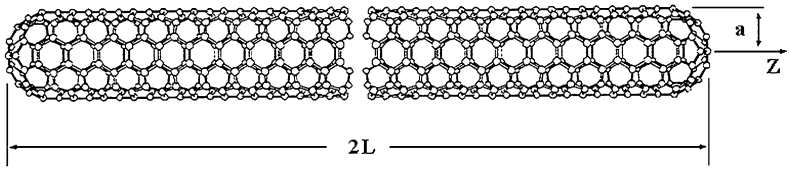

Fig. 2. Profile of armchair nanotube dipole antenna.

MWNTs nanotubes showed polarization sensitivity and wavelength-dependent resonant effects in the optical band [13], and optical Rayleigh scattering measurements on various SWNTs were presented in [14].

In this work, as in [10], metallic carbon nanotube dipole antennas are studied using a Hallén's-type integral equation. However, here we use a quantum mechanical CN conductance function (analogous to the dielectric function), appropriate for optical frequencies, whereas in [10] a semiclassical, low-frequency CN conductance was used. In this respect the underlying model is the same as that used in [12]. This can be considered to be a semiclassical model, since the classical Maxwell's equations are used in conjunction with a quantum conductance. Antenna properties such as the input impedance, current profile, gain and efficiency are presented in the THz, infrared (IR), and optical bands for a common canonical antenna source, the delta-gap voltage source. All units are in the SI system, and the time variation (suppressed) is $e^{j\omega t}$.

II. Formulation

An armchair carbon nanotube having radius a, and oriented along the z axis, is depicted in Fig. 2. The tube is considered to be sufficiently thin ($ka \ll 1$, where k is the free-space wave number) such that circumferentially directed currents can be neglected, as can the azimuthal dependence of the longitudinal current. Therefore, current on the carbon nanotube is $I(z)$, and, as shown in [10], satisfies Pocklington's equation [15]

$$\left(k^2+\frac{\partial^2}{\partial z^2}\right)\int_{-L}^{L} K(z-z')\,I(z')dz' = j4\pi\omega\varepsilon\left(z_{\rm cn}I(z)-E_z^i(z)\right) \quad (2)$$

for $|z| \le L$, where

$$z_{\rm cn}=\frac{1}{2\pi a\sigma_{\rm cn}} \quad (3)$$

is the tube's impedance per unit length, $\sigma_{\rm cn}$ is the conductance (S) of the carbon nanotube, $E_z^i(z)$ is the z component of the incident (source) field, ω is the radian frequency, ε is the permittivity of the surrounding medium ($\varepsilon=\varepsilon_0$ is assumed here), $k=2\pi/\lambda_0$, where the λ_0 is the wavelength of light in empty space at frequency ω, and where the kernel is

$$K(z-z')=\frac{1}{2\pi}\int_{-\pi}^{\pi}\frac{e^{-jk\sqrt{(z-z')^2+4a^2\sin^2(\phi'/2)}}}{\sqrt{(z-z')^2+4a^2\sin^2\left(\frac{\phi'}{2}\right)}}d\phi'. \quad (4)$$

Pocklington's equation (2) does not account for the hemispherical end caps shown in Fig. 2, which are ignored in this analysis. As discussed in [10], (2) is identical in form to the Pocklington equation for an imperfectly conducting metal wire antenna (solid or tubular) [16], with the only difference being that in the case of an ordinary antenna, (3) for the CN would be replaced by the surface impedance per unit length of the metal. In this work, as in [10], the Pocklington form is converted to the Hallén form [15], since it was found that the Hallén form provides more stable numerical results using a simple pulse function discretization. The Hallén's form IE is [10]

$$\int_{-L}^{L}\left(K(z-z')+q(z-z')\right)I(z')dz' = c_1\sin kz+c_2\cos kz - \frac{j4\pi\omega\varepsilon}{2k}\int_{-\infty}^{\infty}E_z^i(z')\sin k|z-z'|\,dz' \quad (5)$$

for $|z| \le L$, where c_1 and c_2 are constants to be determined from the condition $I(\pm L)=0$, and where

$$q(z-z')=2\pi\omega\varepsilon z_{\rm cn}\frac{e^{-jk|z-z'|}}{k}. \quad (6)$$

Integral equation (5) is evaluated using a pulse function expansion, point matching method-of-moments solution [10]. The current is expanded as

$$I(z)=\sum_{n=1}^{N}I_nP_n(z) \quad (7)$$

where I_n are unknown current amplitudes, and $P_n(z)=1$ if $z_n-\Delta/2 \le z \le z_n+\Delta/2$, and $P_n(z)=0$ otherwise, where $z_n=-L+(n-(1/2))\,\Delta$, with Δ being the pulse width, $\Delta=2L/N$. Testing at points $z=z_m$, $m=1,2,\ldots,N$, leads to an $N\times N$ system of equations, from which the pulse amplitudes can be obtained (in all computations presented here, $N=251$ pulses were used, which was found to lead to convergent and stable solutions). Integration techniques described in [17] were employed to evaluate the double integrals associated with the kernel. For the consideration of the transmitting antenna case, the excitation is a delta-gap voltage source [15], $E_z^i(z)=V_0\delta(z)$, where $V_0=1$ V is used here.

Once the antenna current has been obtained, input impedance, gain, efficiency, radiation pattern, and other antenna parameters can easily be determined using well-known methods [15]. In particular, input impedance $Z_{\rm in}$ is computed as

$$Z_{\rm in}=\frac{V_0}{I_0} \quad (8)$$

where V_0 and I_0 are the voltage and current at the feed point. Efficiency is determined from

$$e_r=\frac{P_r}{P_{\rm in}} \quad (9)$$

where

$$P_{\rm in}=\frac{1}{2}\,{\rm Re}\,(Z_{\rm in})\,I_0^2 \quad (10)$$

is the power input to the antenna, and

$$P_r = \frac{1}{2}\,\mathrm{Re}\oint_s \mathbf{E}\times\mathbf{H}^*\cdot d\mathbf{S} \tag{11}$$

is the radiated power. Assuming the nanotube is oriented along the z axis and located in free space [15]

$$P_r = \frac{1}{2\eta}\int_0^{2\pi}\int_0^{\pi} |E_\theta|^2 r^2 \sin\theta d\theta d\phi \tag{12}$$

where

$$E_\theta = j\omega\mu_0 \frac{e^{-jkr}}{4\pi r}\int_{-L}^{L} I(z')\, e^{jkz'\cos\theta} dz' \tag{13}$$

and $\eta = \sqrt{\mu_0/\varepsilon_0}$. Finally, antenna gain is given by

$$G = \frac{2\pi e_r}{\eta}\max_\theta \frac{|E_\theta(\theta)|^2 r^2}{P_r}. \tag{14}$$

It remains to specify the carbon nanotube conductance appearing in (3). Assuming a spatially local response, the π-electron tight-binding quantum conductance is given by [18], [19]

$$\sigma_{\mathrm{cn}}(\omega) = \frac{je^2\omega}{\pi^2\hbar a}\left\{\frac{1}{\omega(\omega-j\nu)}\sum_{s=1}^{m}\int_{1stBZ}\frac{\partial F_c}{\partial p_z}\frac{\partial \mathcal{E}_c}{\partial p_z}dp_z + 2\sum_{s=1}^{m}\int_{1stBZ}\mathcal{E}_c|R_{vc}|^2\frac{F_c-F_v}{\hbar^2\omega(\omega-j\nu)-4\mathcal{E}_c^2}dp_z\right\} \tag{15}$$

where e is the charge of an electron, $\nu = \tau^{-1}$ is the phenomenological relaxation frequency (τ being the relaxation time), $\hbar$ is the reduced Planck's constant, and

$$F_{c,v} = (1 + e^{[(\varepsilon_{c,v}-\mu_{ch})/k_BT]})^{-1} \tag{16}$$

is the equilibrium Fermi distribution function, in which T is the temperature in Kelvin, k_B is Boltzmann's constant, and $\mu_{ch} = 0$ is the chemical potential in graphite. In (15), the electron dispersion relation for armchair CNs is as shown in (17) at the bottom of the page, where $\gamma_0 \approx 2.5 - 3.1$ eV is the approximate range of the overlap integral, $d = 3b/2\hbar$, p_z is the quasi-momentum in the z direction, and where the upper and lower signs refer to the conduction and valence bands, respectively. In the azimuthal direction momentum is quantized due to the finite circumference of the tube, and the summation in (15) is taken over these quantized momentum states. Finally, in (15)

$$R_{vc}(p_z,s) = -\frac{\sqrt{3}b\gamma_0^2}{2\mathcal{E}_c^2(p_z,s)}\sin\left(\frac{d}{\sqrt{3}}p_z\right)\sin\left(\frac{\pi s}{m}\right) \tag{18}$$

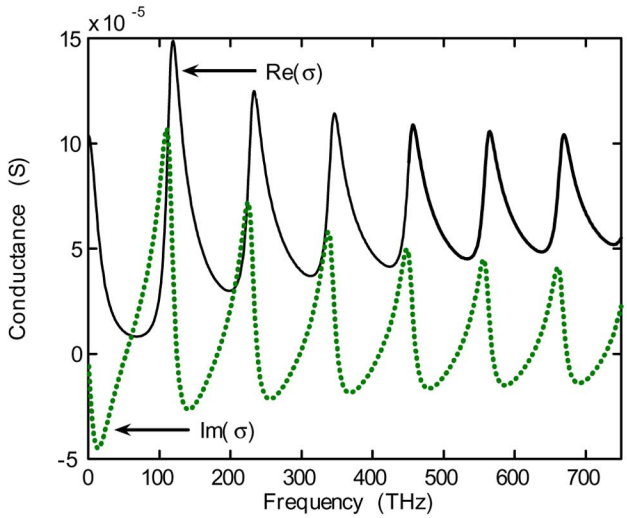

Fig. 3. Real and imaginary parts of σ_{cn} for an armchair nanotube with $a = 2.712$ nm ($m = n = 40$), computed using $\gamma_0 = 3.03$ eV and $\tau = 0.01$ ps.

is the matrix element for armchair CNs. The integral in (15) is performed over the first Brillouin zone (BZ), e.g., from $-2\pi\hbar/\sqrt{3}b$ to $2\pi\hbar/\sqrt{3}b$.

In the low-frequency regime, below optical interband transitions ($\omega < v_F/a$), (15) reduces to the simple expression [18], [20]

$$\sigma_{\mathrm{cn}}(\omega) \simeq -j\frac{2e^2 v_F}{\pi^2\hbar a(\omega-j\nu)} \tag{19}$$

where v_F is the Fermi velocity for a CN (for the range of γ_0 given above, $v_F \simeq 8.1\times10^5 - 1\times10^6$ m/s). Carbon nanotube antenna results based on (19) in the GHz and low THz regime are discussed in [10] and [11].

In Fig. 3, the real and imaginary parts of σ_{cn} for an $a = 2.712$ nm armchair nanotube ($m = n = 40$), computed using $\gamma_0 = 3.03$ eV and $\tau = 0.01$ ps (these value will be discussed later), are shown in the THz, IR, and optical bands. In Fig. 4, the corresponding results are shown for an $a = 0.678$ nm tube ($m = n = 10$).

It can be seen that interband transitions cause spikes in the conductivity in the optical range, associated with van Hove singularities in the density of states [20]. These features lead to similar behavior in the antenna's properties, as discussed below.

III. Discussion of the Model

The presented model has several aspects that warrant discussion.

$$\mathcal{E}_{c,v}(p_z,s) = \pm\gamma_0\sqrt{1+4\cos\left(\frac{\pi s}{m}\right)\cos\left(\frac{d}{\sqrt{3}}p_z\right)+4\cos^2\left(\frac{d}{\sqrt{3}}p_z\right)} \tag{17}$$

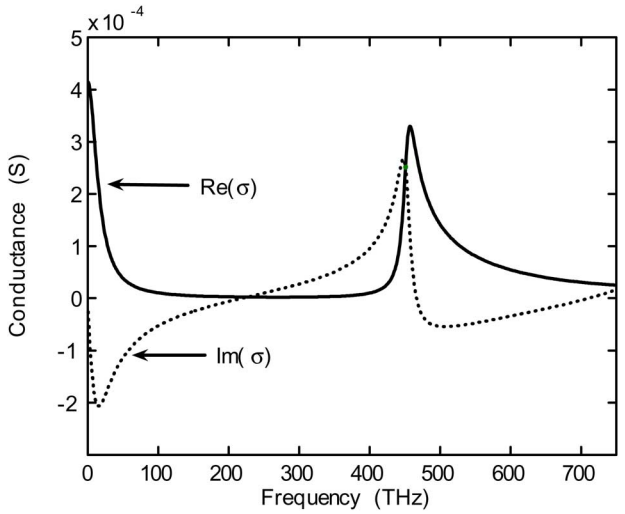

Fig. 4. Real and imaginary parts of $\sigma_{\rm cn}$ for an armchair nanotube with $a = 0.678$ nm $(m = n = 10)$, computed using $\gamma_0 = 3.03$ eV and $\tau = 0.01$ ps.

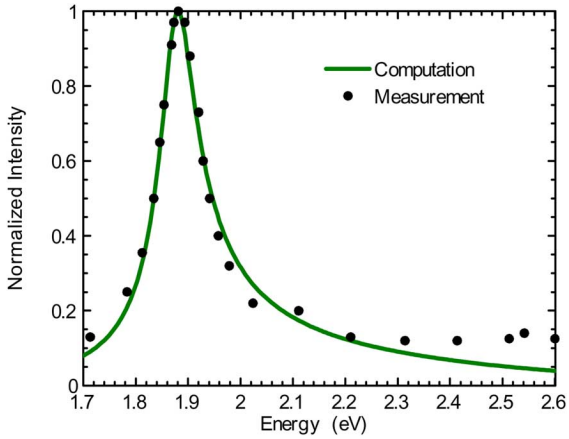

Fig. 5. Comparison between Rayleigh scattering measurements [14] and simulation [computed using (5)] for an $a = 0.678$ nm carbon nanotube $(m = n = 10)$. The simulation used $\tau = 0.0098$ ps and $\gamma_0 = 3.03$ eV. Note that 1.7 eV $\simeq$ 411 THz, and 2.6 eV $\simeq$ 628.7 THz.

A. Integral Equation and Its Numerical Solution

The starting point for deriving the IE (5) is the semiclassical Ohm's law, $\mathbf{J} = \sigma\mathbf{E}$, where the electromagnetic fields are treated classically and the charge carriers are treated quantum-mechanically (via $\sigma_{\rm cn}$, to be described below). The integral equation follows straightforwardly from Ohm's law, and should be valid whenever Ohm's law is valid, subject to being able to neglect circumferentially directed currents and the azimuthal dependence of the longitudinal current on the tube. These restrictions can be lifted by routine electromagnetic analysis, leading to a more complicated set of coupled IEs for the circumferential and longitudinal currents, although this topic is not pursued here since $ka \ll 1$.

The second aspect to consider is the numerical solution of the integral equation. This has been carefully verified by using the surface impedance of an ordinary metal conductor in place of (3), and comparing results with those for imperfectly conducting metallic dipoles [16], [21], [22] (this is further discussed in [10]). Having thus verified the IE and its solution for the metal dipole, one can consider that results for the SWNT should be accurate if $z_{\rm cn}$ provides an appropriate model for the surface impedance of the carbon nanotube.

B. Quantum Conductance Function

The quantum conductance function (15) was developed in [18]–[20], and is based on a π-electron tight binding (TB) model, which has been widely used (see, e.g., [3] and [23]) and includes optical interband transitions. In this model there are two parameters to choose; $\nu = \tau^{-1}$ is the phenomenological relaxation frequency, and γ_0 is the overlap integral. In a tight-binding model of the CN, the location of Van Hove singularities for metallic tubes is given by [20], [24]

$$E_s = 3s\frac{b\gamma_0}{d} \tag{20}$$

where $d = 2a$ is the tube diameter and $s = 1, 2, 3, \ldots$. The energy of optical transitions (dipole-allowed transitions between Van Hove singularities) is $2E_s$, and so γ_0 plays an important role in predicting the location of scattering or absorptance peaks. Reported values of γ_0 cover the range 2.5–3.1 eV, with values at the lower end of the range associated with low-frequency measurements [25], [26], and those at the upper end of the range associated with optical experiments [27], [28]. In this work we use $\gamma_0 = 2.7$ eV for low (GHz and lower THz) frequencies [25], and $\gamma_0 = 3.03$ eV for optical frequencies. The optical value is associated with two-dimensional graphite [3, p. 32], and agrees with the optical value reported in [28], and with a Rayleigh scattering measurement described below.

The second model parameter to choose is the relaxation frequency $\nu = \tau^{-1}$. A wide range of values have been reported in the literature, and it seems that the correct value depends on the energy (frequency) range of interest, and on the tube radius. For example, at dc and low frequencies, ballistic transport has been observed for tubes as long as micrometer lengths; often-quoted mean-free path lengths are in the range 1.3–1.7 μm. Assuming $v_F = 9 \times 10^5$ m/s, this would imply a relaxation time of 1.44–1.88 ps, or relaxation energies in the range of 0.22–0.29 meV. A theoretical estimate resulting from electron interaction with longitudinal acoustic phonons gives $\tau = 1.4$ ps [29], in good agreement with measurements. Furthermore, measurements on high-quality tubes show that ac and dc transport is approximately the same (within a factor of two) up to at least 10 GHz [30], and so through the millimeter wavelength range values of τ on the order of a few picoseconds seem well justified. In [10] $\tau = 3$ ps was used, and this value is used here in the lower THz range.

In the optical range the situation is expected to change from the low-frequency case. Interactions with optical phonons lead to much shorter relaxation times. This is also encountered at low frequencies for high-bias CN transport [31], where high-bias mean-free paths were found to be on the order of 30 nm, leading to a relaxation time of 0.031 ps (20 meV). In the literature different τ values have been used for optical CNs. For example, in [32] (a density-functional method) results are broadened with a Gaussian having full-width half-maximum (FWHM) of 83 meV ($\tau = 0.016$ ps) for band-structure calculations, and 333 meV ($\tau = 0.004$ ps) for optical simulations. In [33] (an *ab initio* many-electron Green's function/Bethe–Salpeter approach), spectra were broadened with a Gaussian factor of

TABLE I
COMPARISON OF THE LOWEST OPTICAL TRANSITION ENERGY E_{11} BETWEEN THE π-ELECTRON TIGHT-BINDING MODEL (π-TB) AND SEVERAL *AB* INITIO THEORIES, AND EXPERIMENT (EXP)

Tube	2a (nm)	$E_{11}^{\pi-TB}$ (eV)	$E_{11}^{ab\ initio}$ (eV)	$E_{11}^{\text{exp.}}$ (eV)	$\%\Delta\ (E_{11}^{\pi-TB}, E_{11}^{\text{exp.}})$	$\%\Delta\ (E_{11}^{\pi-TB}, E_{11}^{ab\ initio})$
$(5,0)$	0.3914	2.20	1.33 [33], 1.2 [32]	1.37 [37]	37% [37]	40% [33], 45% [32]
$(3,3)$	0.4068	6.35	3.17 [33], 2.9 [32]	3.1 [37]	51% [37]	50% [33], 54% [32]
$(10,0)$	0.7829	1.10	0.8 [32]	—	—	27% [32]
$(15,0)$	1.174	2.20	1.6 [32]	—	—	27% [32]
$(10,10)$	1.356	1.90	1.6 [32]	1.88 [14]	1%	16% [32]
$(15,15)$	2.034	1.27	1.1 [32]	—	—	13% [32]
$(20,20)$	2.712	0.95	0.9 [32]	—	—	5% [32]

Note that [32] is not a true *ab initio* method, since an independent electron approximation is assumed in the optical range, which may account for the discrepancies between the results of [32] and [33].

12.5 meV ($\tau = 0.053$ ps), and in [34], 150 meV ($\tau = 0.009$ ps) Lorentzian broadening was used. For semiconducting tubes, photoluminescence measurements showed the influence of tube radius on linewidth (where linewidth decreased with increasing tube radius) [35], but no systematic linewidth measurements seem to be available for metallic tubes.

Most significantly, in [14] Rayleigh scattering measurements were reported for (10,10) tubes, showing a lineshape with a full-width half-maximum of FWHM $\simeq 100$ meV. Converting to frequency and fitting to a Lorentzian lineshape $\Gamma/\left(\pi\left(\Gamma^2+\omega^2\right)\right)$, where FWHM $= 2\Gamma = 2/\tau$, leads to $\tau = 0.0132$ ps, which is in the range described above. This value of τ was fine-tuned in our simulation code to provide a linewidth that is consistent with the experimental result, resulting in $\tau = 0.0098$ ps. With this value for τ, and $\gamma_0 = 3.03$ eV, excellent agreement is found between the simulation result based on (5) and experiment, as shown in Fig. 5 (σ_{cn} for this tube is shown in Fig. 4). For scattering simulations $E_z^i(z) = 1$ over the length of the antenna to simulate a unit-amplitude plane wave normally incident on the CN. The good agreement between simulation and experiment leads confidence in the presented model, to within the adjustable parameters γ_0 and τ.

To summarize the tight-binding modal parameter choices, for lower THz frequencies the values $\gamma_0 = 2.7$ eV and $\tau = 3$ ps will be used, and for the optical range, $\gamma_0 = 3.03$ eV and $\tau = 0.01$ ps. However, it should be kept in mind that the best choice for these parameters will depend on the energy range of interest, and on nanotube structure (e.g., tube radius).

Some further comments should also be made concerning the π-electron tight-binding model. As discussed in [36], the simplest π-electron tight-binding model has been shown to lead to significant errors in optical properties for very small diameter tubes. This fact is not unexpected, since curvature and many-body effects are not accounted for. This is borne out by a comparison between π-TB results, *ab initio* methods, and experimental results. Table I provides a comparison among the different methods and experimental values for the lowest-order optical transition (E_{11}) in several single-wall tubes (for the π-TB results, (20) was used with $\gamma_0 = 3.03$ eV). It can be seen that, as expected, *ab initio* methods generally agree well with experiment, and that predictions of the π-TB model are in error for small tube diameters. However, for larger-diameter tubes the π-TB prediction for E_{11} is in close agreement with *ab initio* results and measurement, as would be expected. In [36] it was stated that for tubes with $d > 1.4$ nm the difference in E_{11} between the π-TB model and better estimates is less than 0.2 eV, which is borne out by the table.

C. Low-Frequency Conduction

Some confidence can be gained in the low-frequency conductance (19) by comparison with another treatment. Assuming $\omega \ll \nu$ and defining the mean-free path as $L_{mfp} = \tau v_F$, then the tube resistance from the conductance (19) is

$$R = \frac{L}{2\pi a \sigma_{\text{cn}}} = \frac{h}{4e^2}\frac{L}{2L_{mfp}} \tag{21}$$

where L is the tube length and $h = 2\pi\hbar$. Alternately, treating a carbon nanotube as a two-channel quantum wire, low bias transport theory (Landauer treatment) indicates that for sufficiently long tube lengths, i.e., tube lengths beyond the ballistic transport regime, CN resistance is given by

$$R = \frac{h}{4e^2}\left(1 + \frac{L}{L_0}\right) \tag{22}$$

where L_0 is a parameter on the order of the mean-free path (see [43, pp. 57–64]). For long tubes where $L \gg L_0$, (21) and (22) agree assuming $L_0 \simeq 2L_{mfp}$. Although the Landauer formula generally applies to dc transport, the correspondence between dc conductance and ac conductance through the GHz range discussed in [30] suggests that (22) may be approximately valid for CNs through the GHz range, where (19) and (21) are applicable, and thus the results of the two different theories may be compared. The correspondence between the results leads to confidence in the presented model, especially since the low frequency part of (15) comes from a semiclassical Boltzmann's equation, and the Landauer formula comes from a transmission probability model of quantum transport near the Fermi energy. Note that since ballistic transport is not contained in (19), the presented IE model should not be used for submicrometer length tubes at extremely low frequencies, where ballistic transport is expected to dominate electron conduction.

D. Delta-Gap Source Model

Finally, a comment on the delta-gap source model is appropriate. This simple source model is extremely common in the antenna field, and leads to predictions that agree well with measurements on ordinary metal antennas for the radiation pattern, input impedance, efficiency, and for other antenna properties of

interest. Usually a two-wire transmission line (carrying the desired signal, or going to a receiver) is connected to the dipole, one wire to each arm of the dipole, possibly through a balun, or for monopole antennas the center conductor of a coaxial cable is extended through a hole in a ground plane and a virtual dipole is formed by image theory. For a CN dipole the same idea would apply, where perhaps another CN, or pair of CNs, would form the incoming transmission line. At this point, the practical issue of how to make the connection to the CN dipole is an open question. However, as the ability to manipulate carbon nanotubes and other nanoscale objects continues to develop rapidly, one can envision that making such connections can be accomplished. Moreover, the predictions based on the delta-gap model should, at least qualitatively, hold for other methods of exciting the dipole. For instance, the presence or absence of resonances, and the effect of interband transitions should be relatively insensitive to the method used to connect the source to the CN. Also, as seen in Fig. 5, the same model works very well for the simulation of CN scattering, although space limitations prevent a thorough presentation of scattering results.

IV. Results

Results are given primarily for a dipole antenna having a half-length of $L = 150$ nm, although dipoles having half-lengths of 50, 500, and 1000 nm are also discussed. The dipole radius is either $a = 2.712$ nm, corresponding to $m = n = 40$ in (1), or $a = 0.678$ nm, corresponding to $m = n = 10$. For the lengths considered the condition $L/a \gg 1$ is satisfied, justifying ignoring circumferential currents (and using a symmetric source allows the neglection of the azimuthal variation of longitudinal currents). Quantum confinement effects in the longitudinal direction can also be ignored, since the Fermi wavelength of electrons in a CN is on the order of a nanometer, and so $L \gg \lambda_F$. The main conclusions of the paper are that for the finite-length carbon nanotube dipoles studied, the antenna exhibits relatively sharp current resonances (due to the finite length of the tube) in the lower THz band according to the velocity factor $v_p \sim 0.01c - 0.003c$, where v_p is the phase velocity of the electromagnetic wave on the carbon nanotube and c is the light velocity in free space. Resonances occur approximately in the frequency range

$$\frac{\nu}{2\pi} \leq f \leq \frac{v_F}{2\pi a} \tag{23}$$

which corresponds to $0.053 \leq f \leq 56$ THz using $\nu^{-1} = 3$ ps and $a = 2.712$ nm. For the (10,10) tube, $0.053 \leq f \leq 225$ THz. In this range, resonance-like input impedances are found, similar to an ordinary metallic dipole antenna. Outside of this frequency range current is strongly attenuated, such that length-dependent resonances do not form. In the range of optical interband transitions, van Hove singularities in the quantum conductance lead to spikes in the input impedance, and in other computed results. Furthermore, due to their small radius, CN antennas have very low efficiencies compared to macroscale antennas.

In Fig. 6 the normalized input impedance of a CN dipole having half-length $L = 150$ nm and $a = 2.712$ nm is shown (in this paper all input impedance results are normalized by the resistance quantum $R_0 = 12.9$ kΩ, and in all plots having two vertical axes, the left and right axis correspond to the real and imaginary part, respectively, of the corresponding quantity). Since a unit amplitude delta-gap source is assumed, Z_{in} is the reciprocal of the current at the center of the antenna. The first resonance occurs at $f_1 = 5.29$ THz, at which, as shown in [10], the current forms approximately a half-wave distribution (resonance is determined by finding the frequency where $\text{Im}\,(Z_{\text{in}}) = 0$). Setting $2L = \lambda_p/2$, where λ_p is a plasmon wavelength, leads to $\lambda_p = 4L = 600$ nm, such that $v_p = \lambda_p f_1 = 0.0106c$. The input impedance at first resonance is 297.97 Ω. The first antiresonance (full-wave resonance) is at $f_2 = 8.09$ THz, leading to $v_p = 0.0081c$, and further (higher order) resonances occur, leading to diminishing v_p; for example, the 12th resonance occurs at 41.72 THz, leading to $v_p = 0.0036c$.

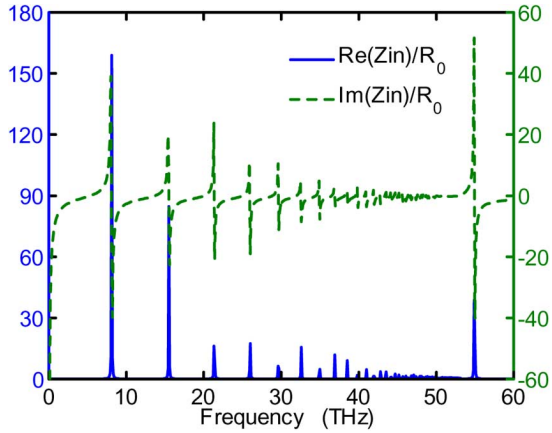

Fig. 6. Input impedance in the THz band for an $L = 150$ nm, $a = 2.712$ nm armchair carbon nanotube antenna, computed using $\tau = 3$ ps, $\gamma_0 = 2.7$ eV.

Other antennas with half-lengths $L = 50$, 500, and 1000 nm and $a = 2.712$ nm were also investigated, and similar behavior was noted. For example, for an $L = 50$-nm dipole, the first resonance and antiresonance occur at $f_1 = 12.67$ THz and $f_2 = 17.14$ THz, respectively. For a 500-nm antenna, the first resonance and antiresonance are at $f_1 = 1.87$ THz and $f_2 = 3.17$ THz, respectively, and for a $L = 1000$-nm antenna, the corresponding values are $f_1 = 1.01$ THz and $f_2 = 1.79$ THz. This leads to phase velocities ranging from $0.0135c$ to $0.0186c$.

As discussed in [10], current resonances are suppressed for frequencies below the relaxation frequency ($F_\nu = \nu/2\pi$; $F_\nu \simeq 53$ GHz assuming $\nu^{-1} = 3$ ps). This is also consistent with measurements in [30], where no resonance behavior was observed (although measurements were only taken up to 10 GHz). The frequency range considered in [10] did not extend beyond a few THz, and so no upper limit on current resonance behavior was observed. In this work it is found that current resonances are also strongly damped above $F_{v_F} = v_F/2\pi a \simeq 56$ THz (for $a = 2.712$ nm), which is in the vicinity of where $\text{Im}\,(\sigma_{\text{cn}})$ crosses the real axis in Fig. 3, and the absolute value of σ_{cn} is at its minimum point. Therefore, for $F_\nu < f < F_{v_F}$, length-dependent current resonances occur, and outside of this range the current is strongly damped.

In order to understand the nature of current resonance damping, it is useful to examine the dispersion curve of the dominant electromagnetic surface-wave mode of an infinite

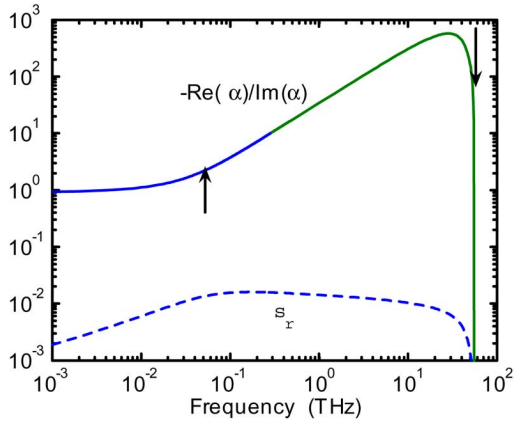

Fig. 7. Dispersion curve for the dominant surface wave on an infinite carbon nanotube having $a = 2.712$ nm (computed using $\gamma_0 = 2.7$ eV and $\tau = 3$ ps). $s_r = v_p/c = k/\alpha_0$ is the normalized phase velocity, and $\mathrm{Re}(\alpha_0)/\mathrm{Im}(\alpha_0)$ indicates the relative loss. The arrows indicate the positions of $\nu/2\pi$ (left-most arrow) and $v_F/2\pi$.

carbon nanotube. In [11] it was shown that the azimuthally independent surface-wave propagation constant of an infinite carbon nanotube satisfies $Z(\alpha) = 0$, where

$$Z(\alpha) = 2\left(\alpha^2 - k^2\right) I_0\left(a\sqrt{\alpha^2 - k^2}\right) K_0\left(a\sqrt{\alpha^2 - k^2}\right) + j4\pi\omega\varepsilon z_{\mathrm{cn}}, \quad (24)$$

I_0 and K_0 are modified Bessel functions, and where α is the propagation constant (a more general dispersion relation is provided in [18]–[20]). In the usual modal theory, the current excited by a source on an infinite cylinder would be expressed as a sum of discrete modes associated with propagation constants α_n, and a continuous summation (integration) of radiation modes [38] (alternately, in a Fourier transform solution, the current would be expressed as a sum of residues and a branch cut contribution [39]). As discussed in [40] and [11], in most situations of interest the dominant contribution to the current comes from the dominant discrete mode. The current on a finite-length tube is also expected to be related to excitation of the dominant discrete mode, which undergoes reflections at the tube ends to form a resonance. In Fig. 7, the dispersion curve for the dominant surface wave ($\alpha = \alpha_0$) on an infinite carbon nanotube having $a = 2.712$ nm is shown, where $s_r = v_p/c = k/\alpha_0$ is the normalized phase velocity, and $\mathrm{Re}(\alpha_0)/\mathrm{Im}(\alpha_0)$ indicates the relative loss. It can be seen that the tube is low-loss over the range $F_\nu < f < F_{v_F}$, which corresponds to $0.053 \leq f \leq 56$ THz (indicated by the arrows) for the tube considered here. Note that this observation was first made in [18]–[20] (see, e.g., [20, Fig. 6.8]).

In Fig. 8, input impedance values are provided for an $L = 150$ nm, $a = 2.712$ nm antenna in the IR and optical regimes. As described above, at these frequencies the CN dipole does not exhibit length-dependent resonances, since current damping is strong. However, the fairly regular set of interband transitions in σ_{cn}, as shown in Fig. 3, leads to oscillating behavior in the corresponding Z_{in} values.

Fig. 9 shows the current distribution on the $L = 150$ nm, $a = 2.712$ nm antenna in the optical regime, at 500 THz. As discussed above, the current is strongly damped, and thus shows no resonance effects (similar current profiles are obtained starting

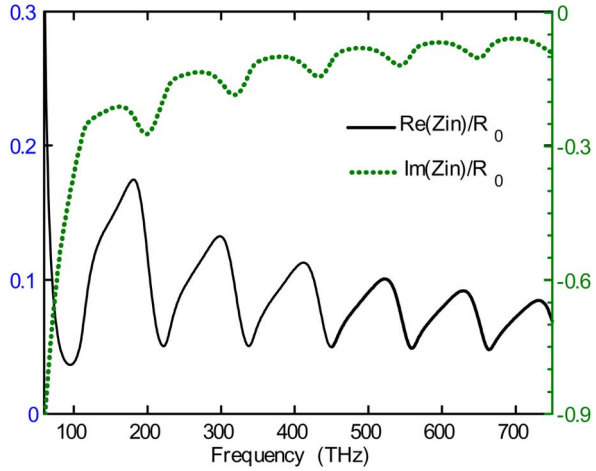

Fig. 8. Input impedance in the IR and optical band for an $L = 150$ nm, $a = 2.712$ nm armchair carbon nanotube antenna (computed using $\gamma_0 = 3.30$ eV and $\tau = 0.01$ ps).

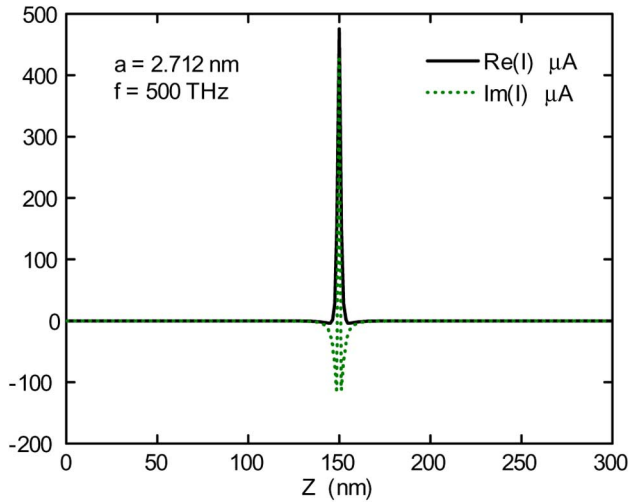

Fig. 9. Current distribution due to a delta-gap source on an armchair carbon nanotube antenna having $2L = 300$ nm and $a = 2.712$ nm, in the optical band, computed using $\gamma_0 = 3.03$ eV and $\tau = 0.01$ ps.

at $f = F_{v_F}$). Fig. 10 is the same as Fig. 9, except for the $a = 0.678$-nm tube.

Although not shown, the radiation pattern for all carbon nanotube antennas considered here is essentially that of a very short dipole (i.e., $E_\theta, H_\phi \propto \sin\theta$). This can be understood physically, since the antenna is very short compared to the free-space wavelength, which is the wavelength of radiation. Radiation into space essentially occurs from an electrically small region around the source concentrated at the origin, and, hence, the pattern is that of a short dipole. Therefore, the directivity of the carbon nanotube antenna is approximately $D \approx 1.5$ [15], although the gain G will be small due to the small value of efficiency $(G = e_r D)$.

Fig. 11 shows gain (14) and efficiency (9) for an $L = 150$ nm, $a = 2.712$ nm nanotube antenna in the THz band.

The gain and efficiency for different length nanotube antennas are similar to that shown in Fig. 11, with the tendency of having more compressed peaks in the gain, and lower peak values, when the antenna length L is longer. For instance, for $L = 50$, 150, 500, and 1000-nm dipoles, in the frequency

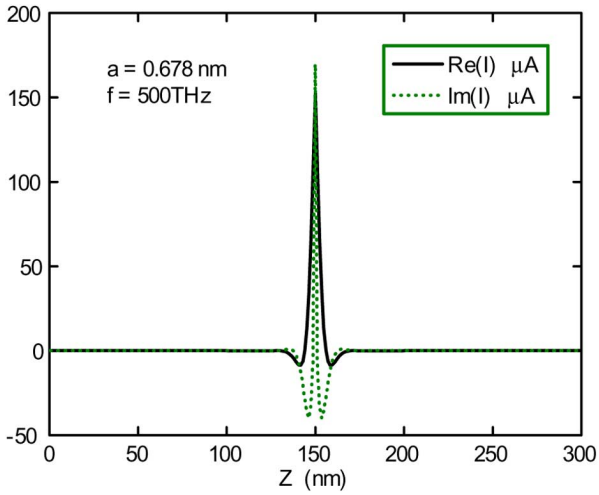

Fig. 10. Current distribution due to a delta-gap source on an armchair carbon nanotube antenna having $2L = 300$ nm and $a = 0.678$ nm, in the optical band, computed using $\gamma_0 = 3.03$ eV and $\tau = 0.01$ ps.

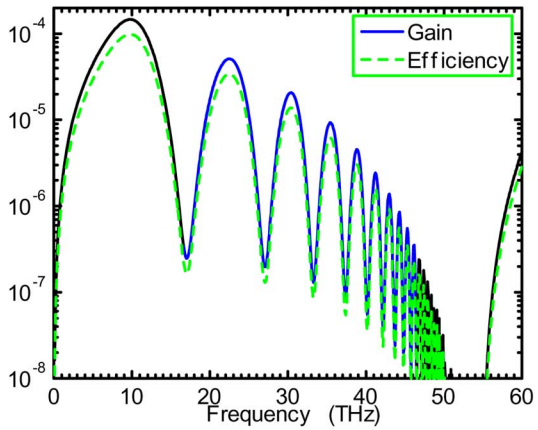

Fig. 11. Gain and efficiency for an $L = 150$ nm, $a = 2.712$ nm nanotube antenna in the THz band, computed using $\gamma_0 = 2.7$ eV and $\tau = 3$ ps.

range up to 40 THz, there are 2, 5, 16, and 32 peaks in the plot of gain or efficiency versus frequency, while the amplitudes of the first efficiency peak are approximately 13×10^{-5}, 9.5×10^{-5}, 4.7×10^{-5}, and 2.8×10^{-5}, respectively. From these results it can be concluded that, unlike classical macroscopic radius metal dipole antennas, the gain and efficiency of carbon nanotube dipoles are very low, due to their extremely small radius.

Fig. 12 shows the gain and efficiency for the same antenna as in Fig. 11, but in the IR and optical regimes. For other length nanotube antennas in this frequency band, e.g., $L = 50,\ 500,$ and 1000 nm, the gain and efficiency behavior are similar, in that they exhibit almost the same numbers of peaks, and peak values, since these are due to interband transitions in $\sigma_{\rm cn}$, rather than current resonances.

V. Summary of Results Predicted by the Model, and Future Work

In light of the simulation results reported in this paper, some comments on the presented model and its predictions are in order.

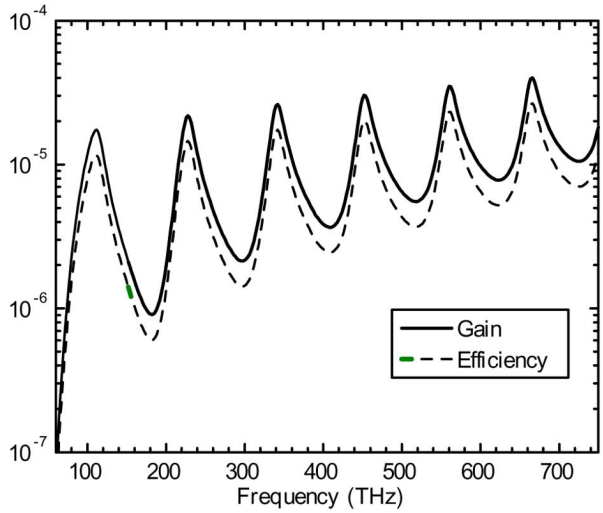

Fig. 12. Gain and efficiency for an $L = 150$ nm, $a = 2.712$ nm nanotube antenna in the IR and optical band, computed using $\gamma_0 = 3.03$ eV and $\tau = 0.01$ ps.

A. Low Frequencies

Using the conductance (19) at low frequencies, in the GHz and low THz range, the presented IE model makes several predictions. First is the absence of current resonances on finite-length tubes below $f = \nu/2\pi$, where $\nu = \tau^{-1}$ is the relaxation frequency. Using $\tau = 3$ ps as discussed previously, we predict the absence of current resonances for $f < 53$ GHz. This is consistent with measurements in [30], where no resonance behavior was observed, although in that work measurements were only taken up to 10 GHz. It remains to verify experimentally that resonances do indeed occur above 53 GHz (more generally, for frequencies above perhaps several tens to several hundreds of GHz, since this value depends on τ). Second, the model predicts that wave velocities along the tube will be approximately $v_p = 0.01c$, so that wavelengths on the tube are approximately a factor of one hundred times smaller than on a perfectly conducting wire. A completely different semiclassical transmission line model for metallic carbon nanotubes (using a quantum capacitance and kinetic inductance) predicts wavelengths on this same order [9], [41], [42], leading to confidence in the model, although, as yet, there are no experimental results to verify this phenomena.

B. IR and Optical Frequencies

In the IR and optical range, the model also makes several predictions. First, above approximately $f = v_F/2\pi a$ current resonances should be strongly damped. This value corresponds to 56 THz for $a = 2.712$ nm, and 225 THz for $a = 0.678$ nm. Scanning near-field optical microscopy (SNOM) may be able to verify or refute this prediction. Second, the model predicts that interband transitions will dominate the antenna properties of individual carbon nanotubes in the optical regime. The Rayleigh scattering results of [14] seem to support this prediction (see Figs. 4 and 5), although additional measurements should be performed on a wide range of tubes. Furthermore, absolute scattering amplitudes can be predicted by our model, and these could be compared to measurements, which could verify not only the number and position of scattering peaks, but also their

amplitudes. Finally, the model presented here shows the same polarization sensitivity (scattered field versus angle of electric field polarization) as was experimentally measured in [14].

Some recent experiments on dense arrays of multiwall carbon nanotubes showed antenna effects (length-dependent resonances, and polarization sensitivity) at optical wavelengths [13]. In that work, resonances were observed corresponding to carbon nanotube lengths $\lambda_0/2$, where λ_0 is the free-space wavelength. This is the usual case for macroscopic radius metal antennas, although this differs from the results presented here, where resonances are suppressed in the optical regime. We conjecture that the observed $\lambda_0/2$ dependent resonances in [13] must be either due to the multiwall nature of the tubes themselves (leading to greatly larger radius values than for SWNTs, and to enhanced conductivity), or to an array effect forming, essentially, an artificial conductive material having thickness $\lambda_0/2$. This problem requires further study.

Finally, we mention that optical transitions in carbon nanotubes may be strongly associated with excitons (bound electron–hole pairs), in both semiconducting and metallic tubes [33], [44], [45]. This would be expected in one-dimensional systems [46], and is not accounted for in the π-electron tight-binding model. Excitonic effects serve to shift the positions of scattering and absorbance peaks, and change the amplitudes of the peaks. In [33], excitonic effects produced an approximately 0.1 eV shift in absorption spectra for a (3,3) tube (predicted using *ab initio* methods), whereas a (5,0) tube exhibited no such shift, and only a minor change in the absorptance peak amplitude. Since here we concentrate on relatively large-radius metallic tubes, excitonic effects may not be very significant, although this is still an open question. Certainly, as demonstrated in Table I, for very small radius tubes (15) should be replaced with an *ab initio* calculation that can account for curvature and many-body effects.

VI. Conclusion

Fundamental properties of dipole antennas formed by finite-length carbon nanotubes have been investigated in the THz, IR, and optical bands via a Hallén's-type integral equation utilizing an axial quantum mechanical conductance. Input impedance, current distribution, gain and efficiency, and radiation patterns have been discussed. Comparisons with other results have been provided, and possible future experimental work has been suggested. The principle conclusions of this study are that carbon nanotube antennas exhibit longitudinal current resonances within a certain frequency range (encompassing GHz and lower THz frequencies), and are strongly damped outside of this range. CN dipoles have high input impedances, which may be beneficial for connecting to nanoelectronic circuits, and exhibit very low efficiencies due to their extremely small radius.

References

[1] I. Iijima, "Helical microtubules of graphitic carbon," *Nature*, vol. 354, pp. 56–58, 1991.

[2] S. Li, Z. Yu, C. Rutherglan, and P. J. Burke, "Electrical properties of 0.4 cm long single-walled carbon nanotubes," *Nano Lett.*, vol. 4, pp. 2003–2007, 2004.

[3] R. Saito, G. Dresselhaus, and M. S. Dresselhaus, *Physical Properties of Carbon Nanotubes*. London, U.K.: Imperial College Press, 2003.

[4] Z. Yao, C. Dekker, and P. Avouris, "Electrical transport through single-wall carbon nanotubes," in *Carbon Nanotubes; Topics in Applied Physics*, M. Dresselhaus, G. Dresselhaus, and P. Avouris, Eds. Berlin, Germany: Springer-Verlag, 2001, vol. 80, pp. 147–171.

[5] S. Li, Z. Yu, S. F. Yen, W. C. Tang, and P. J. Burke, "Carbon nanotube transistor operation at 2.6 GHz," *Nano Lett.*, vol. 4, pp. 753–756, 2004.

[6] J. P. Clifford, D. L. John, L. C. Castro, and D. L. Pulfrey, "Electrostatics of partially gated carbon nanotube FETs," *IEEE Trans. Nanotechnol.*, vol. 3, no. 2, pp. 281–286, Jun. 2004.

[7] G. Pirio, P. Legagneux, D. Pribat, K. B. K. Teo, M. Chhowalla, G. A. J. Amaratunga, and W. I. Milne, "Fabrication and electrical characteristics of carbon nanotube field emission microcathodes with an integrated gate electrode," *Nanotechnology*, vol. 13, pp. 1–4, 2002.

[8] K. G. Ong, K. Zeng, and C. A. Grimes, "A wireless, passive, carbon nanotube-based gas sensor," *IEEE Sensors J.*, vol. 2, no. 2, pp. 82–88, Apr. 2002.

[9] P. J. Burke, S. Li, and Z. Yu, Quantitative theory of nanowire and nanotube antenna performance 2005 [Online]. Available: http://xxx.lanl.gov/abs/cond-mat/0408418

[10] G. W. Hanson, "Fundamental transmitting properties of carbon nanotube antennas," *IEEE Trans. Antennas Propagat.*, vol. 53, no. 11, pp. 3426–3435, Nov. 2005.

[11] ——, "Current on an infinitely-long carbon nanotube antenna excited by a gap generator," *IEEE Trans. Antennas Propagat.*, vol. 54, no. 1, pp. 76–81, Jan. 2006.

[12] G. Y. Slepyan, M. V. Shuba, S. A. Maksimenko, and A. Lakhtakia, "Theory of optical scattering by achiral carbon nanotubes and their potential as optical nanoantennas," *Phys. Rev. B*, vol. 73, pp. 195 416-1–195 416-11, 2006.

[13] Y. Wang, K. Kempa, B. Kimball, J. B. Carlson, G. Benham, W. Z. Li, T. Kempa, A. Rybczynski, and Z. F. Ren, "Receiving and transmitting light-like radio waves: Antenna effect in arrays of aligned carbon nanotubes," *Appl. Phys. Lett.*, vol. 85, pp. 2607–2609, Sep. 2004.

[14] M. Y. Sfeir, T. Beetz, F. Wang, L. Huang, X. M. H. Huang, M. Huang, J. Hone, S. P. O'Brien, J. A. Misewich, T. F. Heinz, L. Wu, Y. Zhu, and L. E. Brus, "Optical spectroscopy of individual single-walled carbon nanotubes of defined chiral structure," *Science*, vol. 312, pp. 554–556, 2006.

[15] R. S. Elliott, *Antenna Theory and Design*. Englewood Cliffs, NJ: Prentice-Hall, 1981.

[16] R. W. P. King and T. T. Wu, "The imperfectly conducting cylindrical transmitting antenna," *IEEE Trans. Antennas Propagat.*, vol. AP-14, no. 5, pp. 524–534, Sep. 1966.

[17] D. H. Werner, J. A. Huffman, and P. L. Werner, "Techniques for evaluating the uniform current vector potential at the isolated singularity of the cylindrical wire kernel," *IEEE Trans. Antennas Propagat.*, vol. 42, no. 11, pp. 1549–1553, Nov. 1994.

[18] G. Y. Slepyan, S. A. Maksimenko, A. Lakhtakia, O. Yevtushenko, and A. V. Gusakov, "Electrodynamics of carbon nanotubes: Dynamic conductivity, impedance boundary conditions, and surface wave propagation," *Phys. Rev. B*, vol. 60, pp. 17 136–17 149, Dec. 1999.

[19] S. A. Maksimenko and G. Y. Slepyan, "Nanoelctromagnetics of low-dimensional structures," in *The Handbook of Nanotechnology—Nanometer Structures—Theory, Modeling, and Simulation*, A. Lakhtakia, Ed. Bellingham, WA: SPIE Press, 2004.

[20] ——, "Electrodynamic properties of carbon nanotubes," in *Electromagnetic Fields in Unconventional Materials and Structures*O. N. Singh and A. Lakhtakia, Eds. New York: Wiley, 2000.

[21] C. D. Taylor, C. W. Harrison, and E. A. Aronson, "Resistive receiving and scattering antenna," *IEEE Trans. Antennas Propagat.*, vol. AP-15, no. 3, pp. 371–376, May 1967.

[22] B. D. Popović and Z. D. Popović, "Imperfectly conducting cylindrical antenna: Variational approach," *IEEE Trans. Antennas Propagat.*, vol. AP-19, no. 3, pp. 435–536, May 1971.

[23] M. F. Lin and K. W. -K. Shung, "Plasmons and optical properties of carbon nanotubes," *Phys. Rev. B*, vol. 50, pp. 17744–17747, 1994.

[24] J. W. Mintmire and C. T. White, "Universal density of states for carbon nanotubes," *Phys. Rev. Lett.*, vol. 81, pp. 2506–2509, 1998.

[25] J. W. G. Wildöer, L. C. Venema, A. G. Rinzler, R. E. Smalley, and C. Dekker, "Electronic structure of atomically resolved carbon nanotubes," *Nature*, vol. 391, pp. 59–62, 1998.

[26] T. W. Odom, J.-L. Huang, P. Kim, and C. M. Lieber, "Atomic structure and electronic properties of single-walled carbon nanotubes," *Nature*, vol. 391, pp. 62–64, 1998.

[27] A. Hagen and T. Hertel, "Quantitative analysis of optical spectra from individual single-wall carbon nanotubes," *Nano Lett.*, vol. 3, pp. 383–388, 2003.

[28] R. Saito, G. Dresselhaus, and M. S. Dresselhaus, "Trigonal warping effect of carbon nanotubes," *Phys. Rev. B*, vol. 61, pp. 2981–2981, 2000.
[29] R. A. Jishi, M. S. Dresselhaus, and G. Dresselhaus, "Electron-phonon coupling and the electrical conductivity of fullerene nanotubes," *Phys. Rev. B*, vol. 48, pp. 11 385–11 389, 1993.
[30] Z. Yu and P. J. Burke, "Microwave transport in metallic single-walled carbon nanotubes," *Nano Lett.*, vol. 5, pp. 1403–1406, 2005.
[31] J. Y. Park, S. Rosenblatt, Y. Yaish, V. Sazonova, H. Üstünel, S. Braig, T. A. Arias, P. W. Brouwer, and P. L. McEuen, "Electron-phonon scattering in metallic single-walled carbon nanotubes," *Nano Lett.*, vol. 4, pp. 517–520, 2004.
[32] G. Y. Guo, K. C. Chu, D. -S. Wang, and C. -G. Duan, "Linear and nonlinear optical properties of carbon nanotubes from first-principles calculations," *Phys. Rev. B*, vol. 69, pp. 205 416-1–205 416-11, 2004.
[33] C. D. Spataru, S. Ismail-Beigi, L. X. Benedict, and S. G. Louie, "Excitonic effects and optical spectra of single-walled carbon nanotubes," *Phys. Rev. Lett.*, vol. 92, pp. 077 402-1–077 402-6, 2004.
[34] E. Chang, G. Bussi, A. Ruini, and E. Molinari, "First-principles approach for the calculation of optical properties of one-dimensional systems with helical symmetry: The case of carbon nanotubes," *Phys. Rev. B*, vol. 72, pp. 195 423-1–195 423-8, 2005.
[35] T. Inoue, K. Matsuda, Y. Murakami, S. Maruyama, and Y. Kanemitsu, "Diameter dependence of exciton-phonon interaction in individual single-walled carbon nanotubes studied by microphotoluminescence spectroscopy," *Phys. Rev. B*, vol. 73, pp. 233 401-1–233 401-4, 2006.
[36] V. N. Popov and L. Henrard, "Comparative study of the optical properties of single-walled carbon nanotubes within orthogonal and nonorthogonal tight-binding models," *Phys. Rev. B*, vol. 70, pp. 115 407-1–115 407-12, 2004.
[37] Z. M. Li, Z. K. Tang, H. J. Liu, N. Wang, C. T. Chan, R. Saito, S. Okada, G. D. Li, J. S. Chen, N. Nagasawa, and S. Tsuda, "Polarized absorption spectra of single-walled 4 Å carbon nanotubes aligned in channels of an $ALPO_4$-5 single crystal," *Phys. Rev. Lett.*, vol. 87, pp. 127 401-1–127 401-4, 2001.
[38] A. W. Snyder and J. D. Love, *Optical Waveguide Theory*. London, U.K.: Chapman & Hall, 1983.
[39] E. Hallén, *Electromagnetic Theory*. New York: Wiley, 1962.
[40] J. A. Stratton, *Electromagnetic Theory*. New York: McGraw-Hill, 1941.
[41] P. J. Burke, "Lüttinger liquid theory as a model of the GHz electrical properties of carbon nanotubes," *IEEE Trans. Nanotechnol.*, vol. 1, no. 3, pp. 129–144, Sep. 2002.
[42] ——, "An RF circuit model for carbon nanotubes," *IEEE Trans. Nanotechnol.*, vol. 2, no. 1, pp. 55–58, Mar. 2003.
[43] S. Datta, *Electronic Transport in Mesoscopic Systems*. New York: Cambridge Univ. Press, 1995.
[44] F. Wang, G. Dukovic, L. E. Brus, and T. F. Heinz, "The optical resonances in carbon nanotubes arise from excitons," *Science*, vol. 308, pp. 838–841, 2005.
[45] G. Dukovic, F. Wang, D. Song, M. Y. Sfeir, T. F. Heinz, and L. E. Brus, "Structural dependence of excitonic optical transitions and bandgap energies in carbon nanotubes," *Nano Lett.*, vol. 5, pp. 2314–2318, 2005.
[46] T. Ogawa, *Optical properties of low-dimensional materials*, T. Ogawa and Y. Kanemitsu, Eds. Singapore: World Scientific, 1995.

Jin Hao (S'05–M'06) was born in Yuci, Shanxi, China, in 1962. He received the B.Sc and M.Sc. degrees from Sichuan University in 1985 and 1988 respectively. Since 2003, he has been working toward the Ph.D degree in the Department of Electrical Engineering, University of Wisconsin, Milwaukee (UWM).

From 1988 to 1999, he was an Assistant Lecturer, Lecturer, Associate Professor, and Professor with Taiyuan University of Technology, Taiyuan, China. From 1999 to 2003, he was with the Department of Electrical Engineering, UWM, as a Visiting Scientist. His interests are in the fields of electromagnetics and antennas, carbon nanotube antennas, and nanotube array characteristics.

George W. Hanson (S'85–M'91–SM'98) was born in Glen Ridge, NJ, in 1963. He received the B.S.E.E. degree from Lehigh University, Bethlehem, PA, in 1986, the M.S.E.E. degree from Southern Methodist University, Dallas, TX, 1988, in and the Ph.D. degree from Michigan State University, East Lansing, in 1991.

From 1986 to 1988, he was a development engineer with General Dynamics in Fort Worth, TX, where he worked on radar simulators. From 1988 to 1991, he was a research and teaching assistant in the Department of Electrical Engineering at Michigan State University. He is currently Associate Professor of Electrical Engineering and Computer Science at the University of Wisconsin, Milwaukee. His research interests include nanoelectromagnetics, mathematical methods in electromagnetics, electromagnetic wave phenomena in layered media, integrated transmission lines, waveguides, and antennas, and leaky wave phenomena.

Dr. Hanson is an Associate Editor for the IEEE TRANSACTIONS ON ANTENNAS AND PROPAGATION, and is a member of URSI Commission B, Sigma Xi, and Eta Kappa Nu.